Eur. Phys. J. C manuscript No.
(will be inserted by the editor)

New methods to reconstruct $X_{\max}$ and the energy of gamma-ray air showers with high accuracy in large wide-field observatories

R. Conceição[1,2], L. Peres[1,2] M. Pimenta[1,2], B. Tomé[1,2]

[1] LIP, Av. Prof. Gama Pinto, 2, P-1649-003 Lisbon, Portugal
[2]Instituto Superior Técnico (IST), Universidade de Lisboa, Av. Rovisco Pais 1, 1049-001, Lisbon, Portugal

arXiv:2010.11390v2 [hep-ph] 15 Jan 2021

Received: date / Accepted: date

Abstract Novel methods to reconstruct the slant depth of the maximum of the longitudinal profile ($X_{\max}$) of high-energy showers initiated by gamma-rays as well as their energy (E_0) are presented. The methods were developed for gamma rays with energies ranging from a few hundred GeV to ~ 10 TeV. An estimator of $X_{\max}$ is obtained, event-by-event, from its correlation with the distribution of the arrival time of the particles at the ground, or the signal at the ground for lower energies. An estimator of E_0 is obtained, event-by-event, using a parametrization that has as inputs the total measured energy at the ground, the amount of energy contained in a region near to the shower core and the estimated $X_{\max}$.

Resolutions about 40 (20) g/cm^2 and about 30 (20)% for, respectively, $X_{\max}$ and E_0 at 1 (10) TeV energies are obtained, considering vertical showers. The obtained results are auspicious and can lead to the opening of new physics avenues for large wide field-of-view gamma-ray observatories. The dependence of the resolutions with experimental conditions is discussed.

Keywords High Energy gamma rays · Wide field observatories · Depth of the shower maximum · energy distribution at the ground · Primary energy reconstruction resolution

1 Introduction

High energy cosmic and gamma rays entering the Earth atmosphere originate Extensive Air Showers (EAS) which may be characterised by the distributions of the number of shower particles N as a function of the traversed atmospheric slant depth X (longitudinal profiles) and/or by the distributions of the particles arriving at the ground level as a function of the distance to the shower core (Lateral Density Function - LDF).

The longitudinal development of gamma-ray initiated showers was historically described by Rossi and Greisen diffusion equations [1] being the well known Greisen [2] and Gaisser-Hillas [3] functions approximate solutions. It can be demonstrated that these functions lead to a quasi-universal shape [4]. This universality can be shown by representing the shower longitudinal profile in the plane ($N' = N/N_{\max}$, $X' = X - X_{\max}$), where $X_{\max}$ is the slant depth of the maximum of the profile and $N_{\max}$ is the number of the shower particles at that depth. In this reference frame, the profile may be seen as a slightly asymmetric Gaussian with variable width and is essentially insensitive to variations induced by the depth of the first interaction [5]. However, at TeV energies or below, the fraction of events where the longitudinal profile do not follow the quasi Gaussian shape may not be negligible. A few of the profiles will have a slower decrease after $X_{\max}$ or even having a double peak structure. These anomalous shower profile structures are associated with interactions where particles travel several radiation/interaction lengths before interacting, or when one of the sub-products of the interaction takes nearly all of the available energy.

Imaging Air Cherenkov Telescopes (IACTs) collect Cherenkov light produced by the EAS and are able, due to their size, intensity, and orientation of the projected image in the camera focal plane, to reconstruct the energy and the direction of the primary gamma-ray. Typical energy resolution of $15\% - 20\%$ are often quoted for TeV gammas and zenith angles of about 20°, for instance, the resolution of MAGIC-II was measured to be 15% [6].

[a]e-mail: ruben@lip.pt

Ground-based gamma-ray observatories sample the particles (mainly electrons and photons) arriving at the ground level and from their time and position distributions can determine, with reasonable accuracy, the shower core position and the direction of the primary gamma-ray. The determination of the shower energy has, however, a large uncertainty. Indeed, energy resolutions of the order of several tens of percent are often quoted. For instance, in [7] using a Likelihood fit with Monte Carlo template distributions, the energy reconstruction resolution at 10 TeV is $\sim 50\%$ and the HAWC collaboration has recently reported an improved energy resolution of 40% at the same energy using a neural network analysis [8].

One of the main limiting factors in the reconstruction of the primary energy for ground arrays is the uncertainty on the position of the first interaction in the atmosphere. Contrary to IACT arrays, there is no direct measurement for ground arrays of the contents of the EAS in the region of the shower maximum, and therefore the shower development stage is unknown. In fact, for showers induced by gamma-rays, with the same energy and zenith angle, the number of particles at the ground is expected to increase with $X_{\max}$. The previous statement is not absolute as the width of the longitudinal profile is also an important factor to determine not only the total energy at the ground but also the fraction of this energy present in the region of the shower core. A larger shower profile width will, for the same $X_{\max}$, have larger energy at the ground and a more substantial fraction of energy in the region near the core. Indeed, it is possible to establish, at fixed primary energy, a correlation between the fraction of the energy in the region near the core and the total energy carried by electromagnetic particles (photons, electrons and positrons) that reach the ground ($S_{\rm em}$).

The energy measured by a detector array with electromagnetic calorimetric capabilities, like Water Cherenkov Detectors, is by definition highly correlated with $S_{\rm em}$. Such correlation is explored to built an estimator of $S_{\rm em}$ (section 2).

$X_{\max}$ is not easily estimated at ground gamma-ray observatories. However, at very high energies in cosmic rays experiments, correlations between $X_{\max}$ and the distribution of the arrival times of the particles at the ground in each event, have been established [9]. Such correlations are exploited to build an estimator of $X_{\max}$ (section 3).

An innovative method for the reconstruction of the primary energy of each event, having as inputs the total measured energy at the ground, the fraction of this energy measured in the region near the shower core and the estimated $X_{\max}$, is then presented (section 4).

Finally, the applicability of such method in realhistogrammed large wide-field gamma-ray observatories is discussed (section 5).

All the present results were obtained using CORSIKA (version 7.5600) [10] to simulate vertical gamma-ray showers assuming an observatory at an altitude of 5200 m a.s.l. The primaries, with energies between 250 GeV and 15 TeV, were injected following an energy spectrum of E^{-1}, which guarantees high enough statistics over the whole simulated energy range. It was used as hadronic interaction model for low and high energy, FLUKA and QGSJET-II.04, respectively, although the choice of these models has little impact on the simulation of electromagnetic showers. The total energy of electromagnetic shower particles was recorded at the observation level and histogrammed in radial bins of 4 meters. This would mimic a calorimeter detector compact array, where the station unit covers an area of $\sim 12\,\mathrm{m}^2$. A full study including different zenith angles, detailed simulations of realistic detectors, a wider energy range and also its application to hadronic induced showers, is out of the scope of this work. The main focus of this article is the explanation of the newly proposed method to achieve an accurate energy reconstruction of gamma-ray air showers between several hundreds of GeV and a few TeV. This is the most challenging energy region for this kind of experiments. In addition to the uncertainty on the shower stage, the number of secondary shower particles that reach the ground is reduced when comparing with energies of the order of tens of TeV, undermining the capability to reconstruct the shower quantities. A first glance on its potential is given.

2 Energy distribution at the ground

The density of the shower particles arriving at the ground, as a function of the distance to the shower core, is steeper in the region near the core and flatter at larger distances. This distribution is usually parametrized using the NKG (Nishimura-Kamata-Greisen) formula [11]. The particle density at a given distance from the air shower axis is often used to obtain an estimator of the primary energy, trying to find a region less sensitive to the fluctuations in the shower development, to the primary nature and to array sampling effects. For instance, in the Tibet Air Shower Array, this distance was found to be 50 m [12].

The energy distribution at the ground as a function of the distance r to the core position and its cumulative function, $F(r)$, are shown in figure 1 for an event with $S_{\rm em} = 96.5\,\mathrm{GeV}$, $E_0 = 1165.9\,\mathrm{GeV}$ and $X_{\max} = 334\ \mathrm{g\,cm^{-2}}$.

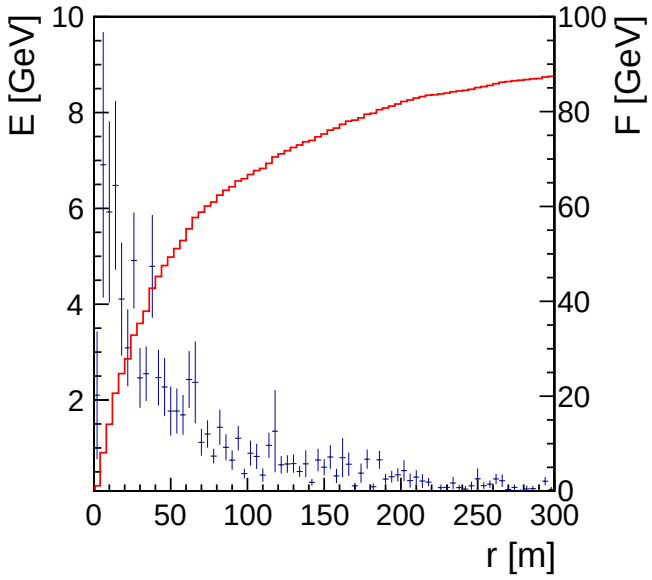


Figure 1 The energy distribution at the ground for one event with $S_{\rm em}$ = 96.5 GeV, E_0 = 1165.9 GeV and $X_{\rm max}$ = 334 g cm^{-2}. Also shown the respective cumulative function $F(r)$.

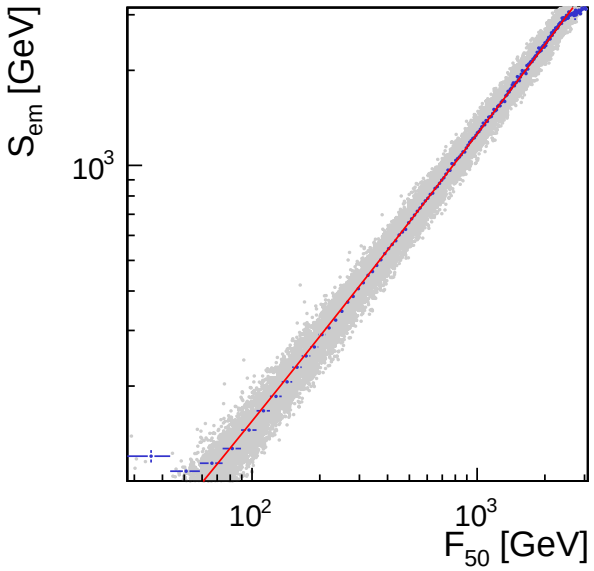


Figure 2 Correlation of the electromagnetic energy deposited at the ground, $S_{\rm em}$, with F_{50}, the energy deposited at the ground within a radius of 50 m from the core position (see text for the simulation details).

The strategy followed in this article is different from one usually employed by shower array experiments [8, 13]. Instead of using the shower particle density at the ground at some optimized distance from the shower core, the aim is to characterize the shower development through two variables that will be then used to predict, event by event, the calibration factor between the gamma-ray energy (E_0) and the electromagnetic energy arriving at the ground ($S_{\rm em}$).

$X_{\rm max}$, whose estimator will be discussed in the next section, is naturally one of these variables. The other, f_{20}, is defined as the ratio between the energy at the ground collected at a distance less than 20 m from the shower core and the total energy at the ground. This parameter will be the main responsible for the improvement of the energy resolution reached in this article. The rationale of this second variable was already introduced in the previous section. For a given E_0 and $X_{\rm max}$, the development of the shower between the $X_{\rm max}$ region and the ground level will strongly determine f_{20}.

An estimator of $S_{\rm em}$, designated as A_0, may be obtained using the correlation between $S_{\rm em}$ and $F_{r_0} \equiv F(r_0)$, being r_0 a reference distance. In any case, r_0 should be greater than 20 m to ensure a good correlation, and lower than some tens of meters to ensure a high number of events where the event footprint, with $r < r_0$, is fully contained within the compact array region of the observatory. For the purpose of this article, in the following $r_0 = 50$ m is used.

The correlation between $S_{\rm em}$ and F_{50} is shown in figure 2 and A_0 is parametrized as:

$$A_0 = F_{50} + G\,F_{50}^{\delta} \qquad (1)$$

where G and δ are free positive parameters. This parametrization ensures, by construction, that A_0 is always greater then F_{50}. With A_0 and F_{50} in GeV, the best values found to be for $G = 1.63\,\mathrm{GeV}^{0.28}$ and $\delta = 0.72$. The result is shown as a red curve in figure 2.

The obtained resolutions and bias[1] of A_0 are summarized in figure 3, as a function of $S_{\rm em}$. As a reference a primary energy of 1 TeV and 10 TeV corresponds to a mean value of $S_{\rm em}$ of 115 GeV and 3 TeV, respectively (see figure 10). Thus, resolutions of about 12% and 5% are found at primaries energies of 1 TeV and 10 TeV, respectively, while the bias is consistently in the order of a few percent.

In principle, a better estimator of $S_{\rm em}$ can be obtained using a continuously measured distribution of $F(r)$ and not just a single measurement at r_0. With

[1] In this work, the bias and resolutions of the estimator, $\hat{x}$, of variable, x, are taken fitting a gaussian function to the residuals, $(1-(\hat{x}/x))$. The bias and the resolution corresponds to the mean and the sigma parameter of the fitted gaussian, respectively.

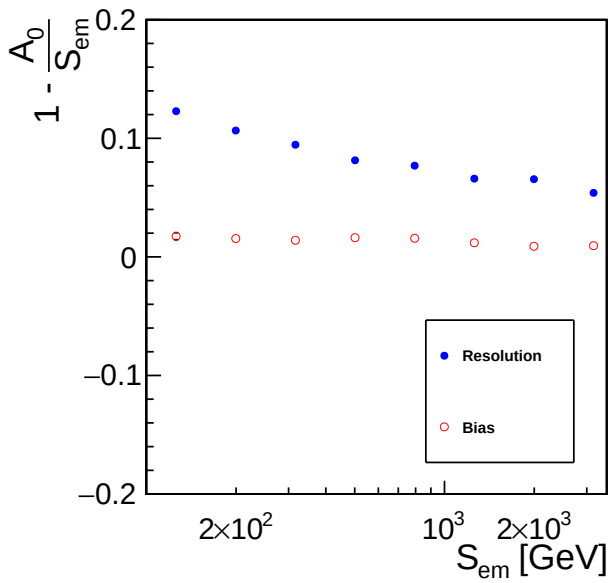


Figure 3 Bias and the relative resolution of the estimator A_0 of the energy deposited at the ground, defined in equation 1, as a function of the energy deposited at the ground, $S_{\rm em}$ (see text for the simulation details).

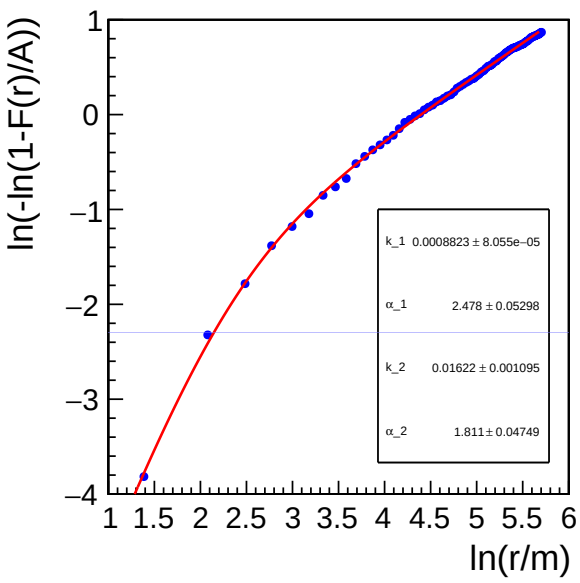


Figure 4 The blue points represent the binned cumulative function of the electromagnetic energy distribution at the ground of the event shown in figure 1, assuming $A_1 = S_{\rm em}$. The red line is the best fit to these data points using the parametrization defined in equation 2.

this purpose, $F(r)$, which is a smooth and continuous function, was parametrized as:

$$F(r) = A_1 \left[1 - \exp\left(-\frac{k_1 r^{\alpha_1}}{1 + k_2 r^{\alpha_2}}\right)\right]. \quad (2)$$

The parameter A_1 is the $S_{\rm em}$ estimator while the terms $k_i r^{\alpha_i}$ describe the steepness of the function, being $k_1 > 0$, $\alpha_1 > 0$ and $0 \leq k_2 \leq 1$, $0 \leq \alpha_2 < \alpha_1$.

In the limits $r \to 0$ and $r \to \infty$ this parametrization becomes,

$$F(r)/A_1 = [1 - \exp(-k_1 r^{\alpha_1})] , \quad (3)$$

and,

$$F(r)/A_1 = \left[1 - \exp\left(-\frac{k_1}{k_2} r^{(\alpha_1 - \alpha_2)}\right)\right], \quad (4)$$

which have the form of Weibull cumulative distribution functions [14].

Indeed, as an example, it is shown in figure 4 that, in the plane $(\ln(-\ln(1-(F(r)/A_1))), \ln(r))$ and assuming $A_1 = S_{\rm em}$, the cumulative distribution function of the event shown in figure 1 (blue points) is well described by the above parametrization.

In this plane a pure Weibull function is just a straight line while to describe this event two straight lines are needed due the transition between the two regimes in the region 20 m − 30 m ($\ln(r/m) = 3$ - 3.5). This transition region matches the known behaviour of the energy distribution at the ground with a higher concentration of energy in the core region. Similar fits to a large number of events and whose cumulative functions correspond to quite different steepness in the core region are equally very good.

In a real event $S_{\rm em}$ is not known and the parameter A_1, as well as the parameters k_1, α_1, k_2 and α_2, have to be fitted. However, it was found that the convergence of this fit is not trivial, as A_1 is highly correlated with combinations of the other parameters, and thus elaborated fit strategies will have to be defined, which is beyond the scope of the present article. In these terms A_0 will be the $S_{\rm em}$ estimator used hereafter.

The variable f_{20} is then defined as F_{20}/A_0. The choice of 20 m for the definition of this variable is a compromise which should be optimized for each specific experiment. Nevertheless, its value should be typically between 15 m and 30 m. Lower values will conflict with the possible experimental resolutions on the shower core, higher values will enter in the region where the cumulative function has a slower increase and also where, for events with the core nearer to the border of

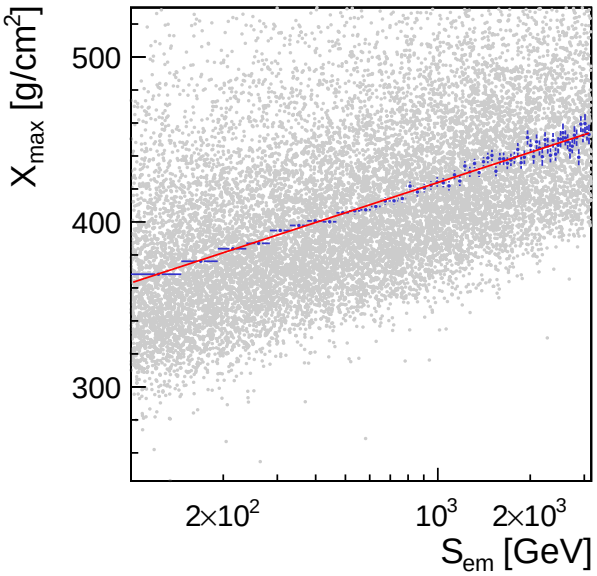


Figure 5 Correlation of the slant depth of the maximum of the air shower longitudinal profile, $X_{\rm max}$, with the energy deposited at the ground, $S_{\rm em}$ (see text for the simulation details).

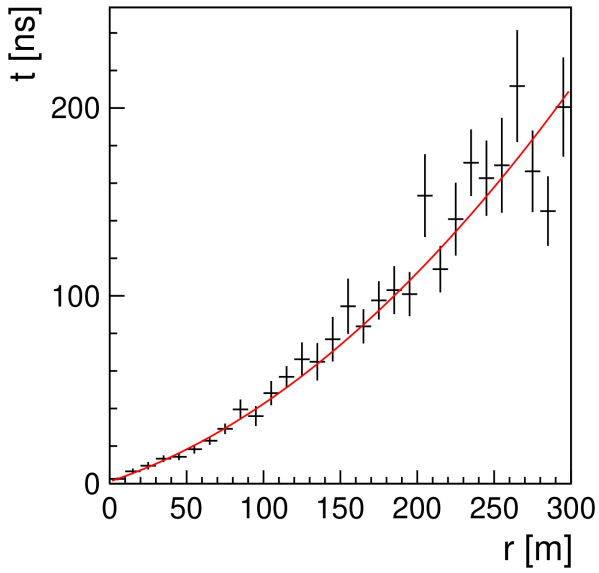


Figure 6 Arrival time as a function of the distance to the core for an event with $X_{\rm max} = 339\,{\rm g\,cm^{-2}}$ and $E_0 = 1.3\,{\rm TeV}$. The line correspond to a quadratic fit as explained in the text with its $\chi^2/{\rm ndf} = 0.93$ (see text for the simulation details).

the compact region of the array, there will be no direct measurement of the cumulative function.

3 $X_{\rm max}$ reconstruction and resolution

A first order estimation of $X_{\rm max}$ may be obtained observing that the mean value of $X_{\rm max}$ increases with the increase of the electromagnetic energy arriving at the ground ($S_{\rm em}$), reflecting the increase of the shower size with the primary energy. This correlation is demonstrated in figure 5 where $X_{\rm max}$ is represented as a function of $S_{\rm em}$. It is then possible to parametrize $X_{\rm max}$ as a function of $S_{\rm em}$ as:

$$X^0_{\rm max} = B_0 + \gamma_0 \log(S_{\rm em}/{\rm GeV}). \quad (5)$$

with B_0 and γ_0 parameters tuned to describe the mean behaviour. The best achieved parameterization is shown in figure 5 as a red filled curve (corresponding to $B_0 = 237.1\,{\rm g\,cm^{-2}}$ and $\gamma_0 = 62.3\,{\rm g\,cm^{-2}}$).

A more precise estimate of $X_{\rm max}$ may be obtained exploring the fact that the shower front at the ground is a curved surface [15]. Ideally, if the shower particles were produced in a single point located along the shower axis, for instance at the $X_{\rm max}$, this surface will be spherical, assuming that all the particles travel approximately with the speed of light. The arrival time in each surface station would then change accordingly as a function of the distance to the shower core and with the primary particle direction. Using a simple geometrical fit, the $X_{\rm max}$ position would be reconstructed straightforwardly, with an accuracy that would mainly depend on the time resolution of the stations.

In reality, the geometry is more complex, but nevertheless, it is possible to establish a clear correlation between $X_{\rm max}$ and the arrival time distribution of particles at the ground. As an example in figure 6 this correlation is shown for an event with $X_{\rm max} = 339\,{\rm g\,cm^{-2}}$ and $E_0 = 1.3\,{\rm TeV}$. It was found that most of the events can be described by a quadratic polynomial of the form,

$$t = a + b\,r + c\,r^2. \quad (6)$$

In fact, the application of the above equation to the time profiles as a function of the distance to the shower core leads to a well behaved χ^2/ndf distribution with the distribution maximum peaking at ~ 1.2.

The parameter of the quadratic term of the polynomial, c, is strongly correlated with $X_{\rm max}$ (figure 7). The parameter b is nearly independent of $X_{\rm max}$, and a is associated with the event initial time, T_0, usually set to zero when the shower front reaches the shower core position. The dependence of c with $X_{\rm max}$ can be understood if one assumes that most of the particles

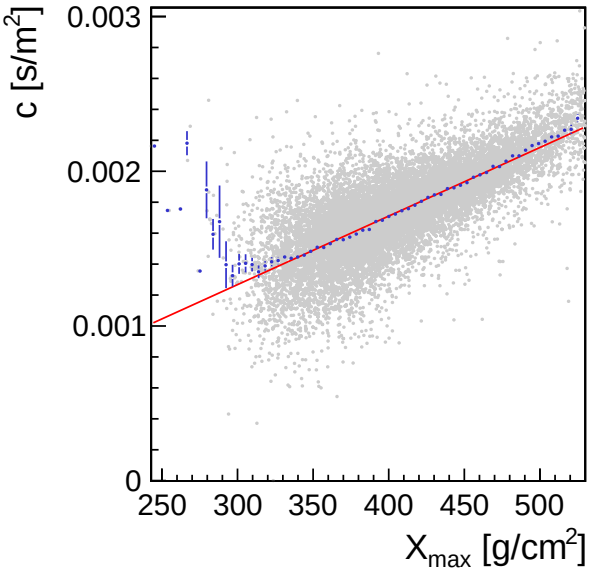


Figure 7 Correlation of the c curvature parameter with the slant depth of the maximum of the longitudinal profile, $X_{\max}$. See equation 6 for a definition of the c parameter (see text for the simulation details).

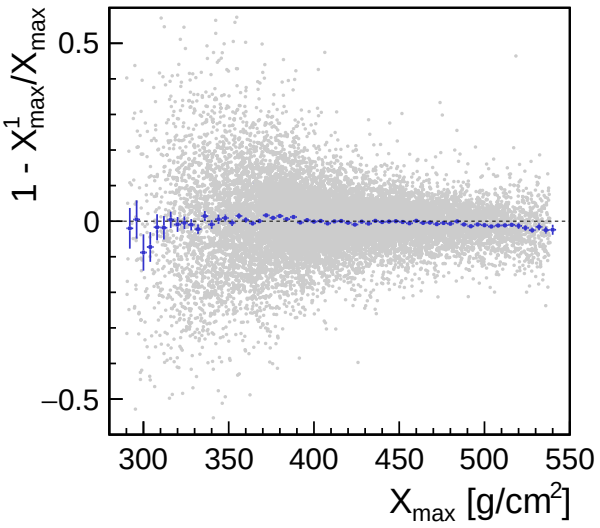


Figure 8 Normalized deviation of the estimator $X^1_{\max}$, defined in equation 7, from the real $X_{\max}$, as a function of $X_{\max}$ (see text for the simulation details).

produced in a shower come from $X_{\max}$ and the shower particles propagate as spherical front. This is of course an approximation but figure 7 supports it and it helps to build some intuition.

Hence, it is possible to parametrize $X_{\max}$ as a function of c using:

$$X^1_{\max} = B_1 + \gamma_1\, c. \tag{7}$$

B_1 and γ_1 are parameters tuned to describe the profile shown in figure 7. The best achieved parametrization is shown by the red curve, with $B_1 = 11.2\,\mathrm{g\,cm^{-2}}$ and $\gamma_1 = 2.28 \times 10^9\,\mathrm{g\,s^{-1}}$.

$X^1_{\max}$ does not show any relevant bias even for low $X_{\max}$, as shown in figure 8. Nevertheless, in a few cases, particularly at lower energies where the number of particles arriving at the ground is small, the fit may converge to c values leading to non-physical values of $X_{\max}$. In practice, whenever the estimation of $X_{\max}$ from the fit indicates values lower than $300\,\mathrm{g\,cm^{-2}}$, the first order estimation $X^0_{\max}$ is used.

The obtained resolutions as a function of S_{em}, both for $X^0_{\max}$ and $X^1_{\max}$, are summarized in figure 9. Resolutions of about $40\,\mathrm{g/cm^2}$ and $20\,\mathrm{g/cm^2}$ were found for primaries energies of 1 TeV and 10 TeV, respectively.

The two resolutions are similar in the region $A_0^{\mathrm{crX}} \approx 400 - 600\,\mathrm{GeV}$. To be on the safe side, avoiding possible tail effects, we set $A_0^{\mathrm{crX}} = 600\,\mathrm{GeV}$. Therefore, the estimator of $X_{\max}$, designated as $X^R_{\max}$ is defined as:

$$X^R_{\max} = \begin{cases} X^1_{\max} & \text{if } A_0 > A_0^{\mathrm{crX}} \\ & \text{and } X^1_{\max} > 300\,\mathrm{g\,cm^{-2}} \\ X^0_{\max} & \text{otherwise} \end{cases} \tag{8}$$

4 Energy reconstruction and resolution

In electromagnetic showers, the production of muons, either via the photo-production of mesons or by the direct creation of muon pairs is quite small [16] and can thus be neglected in the global accounting of the shower energy.

On the other hand, the logarithm of the electromagnetic energy deposited in the atmosphere ($E_0 - S_{\mathrm{em}}$) is linearly correlated with the logarithm of the energy deposited at the Earth surface (S_{em}), as shown in figure 10.

It is then possible to parametrize E_0 as a function of S_{em} as:

$$E_0^{(1)} = S_{\mathrm{em}} + C\,(S_{\mathrm{em}})^{\beta}, \tag{9}$$

where C and β are free positive parameters. This parametrization ensures, by construction, that $E_0^{(1)}$ is always greater then S_{em}. The best values found for C

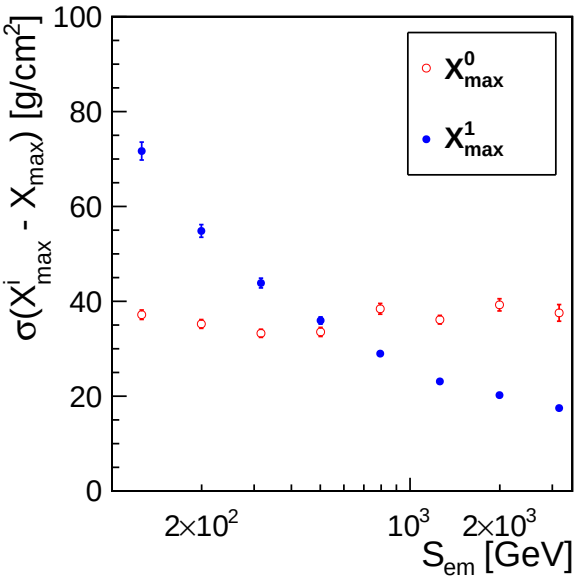


Figure 9 Resolution of the $X_{\rm max}$ estimators $X^0_{\rm max}$ and $X^1_{\rm max}$ as a function of $S_{\rm em}$ (see text for the simulation details).

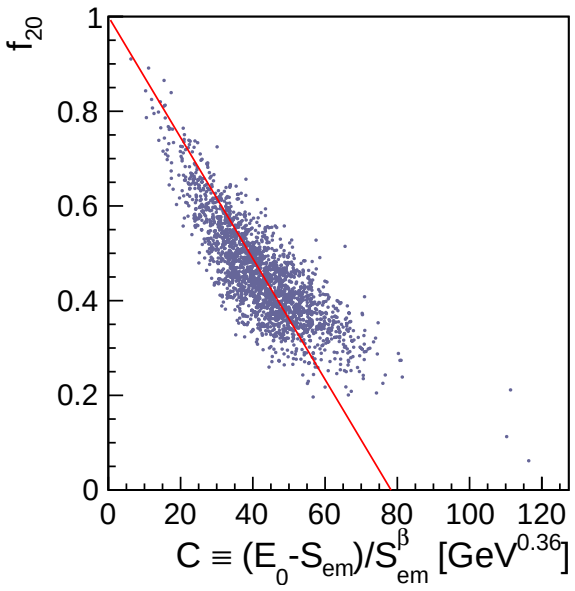


Figure 11 Correlation of the variable f_{20}, as defined in the text, with the calibration coefficient C, for events with $S_{\rm em} \sim 200\,{\rm GeV}$ and $X_{\rm max} \sim 350\,{\rm g/cm^2}$ (see text for the simulation details).

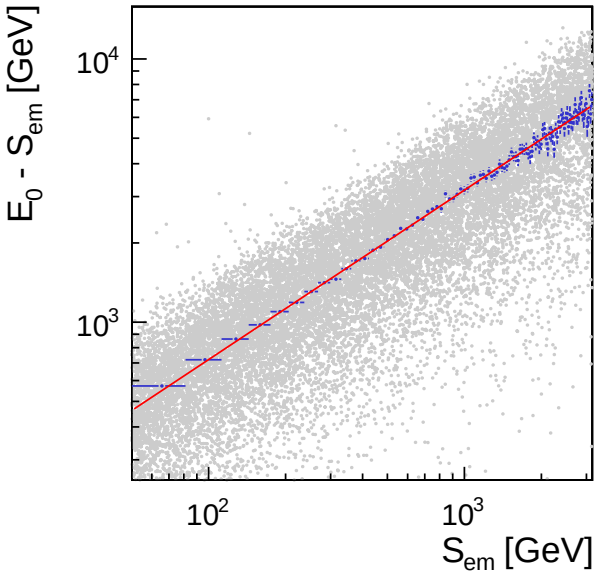


Figure 10 Correlation of the energy deposited in the atmosphere (primary energy minus the electromagnetic energy at the ground), $E_0 - S_{\rm em}$ with the energy deposited at the ground $S_{\rm em}$. The line corresponds to the best parametrization (see text for details).

and β are $37.2\,{\rm GeV}^{0.36}$ and 0.64, respectively. The result is shown as a red curve in figure 10.

Using the above parametrization and A_0 (see section 2) as the estimator of $S_{\rm em}$, it is possible to make a first energy reconstruction considering an *ideal* detector[2]. An energy resolution of about 40% is obtained at 1 TeV.

The coefficient C, in this first calibration attempt, is a constant. However, C can be shown to be correlated with f_{20}, $X_{\rm max}$ and $S_{\rm em}$. Indeed, it is shown in figure 11 a striking correlation between f_{20} and $C = (E_0 - S_{\rm em})/(S_{\rm em})^\beta$, for events with $S_{\rm em} \in [100; 250]\,{\rm GeV}$ and $X_{\rm max} \in [330; 385]\,{\rm g\,cm^{-2}}$. The line in the figure is the best linear parameterization imposing that for $C = 0$ (no energy deposited in the atmosphere), $f_{20} = 1$ (all the deposited at the ground is at a distance lower than 20 m from the shower core position).

The set of the correlation lines (f_{20}, C) for several $X_{\rm max}$ ranges and $S_{\rm em} \sim 200\,{\rm GeV}$, are shown in figure 12. There is a linear monotonous decrease of the slope m of these lines with the increase of $X_{\rm max}$. In figure 13 the obtained m are represented as a function of $X_{\rm max}$ for different bins of $S_{\rm em}$ together with the best linear parametrization for each $S_{\rm em}$ bin.

The extrapolation of these lines for $X_{\rm max} = 0$ points to a non-physical small positive value of m ($b_m \sim 0.011\,{\rm GeV}^{-0.36}$), which means that this linear model is no longer valid for $X_{\rm max} < 200\,{\rm g\,cm^{-2}}$,which is far below the relevant $X_{\rm max}$ region for this art-

[2]By *ideal* detector it is assumed a detector able to accurately collects all the energy of electromagnetic particles reaching the station. The impact of having a *real* calorimetric detector such as a water Cherenkov detector is addressed in section 5.

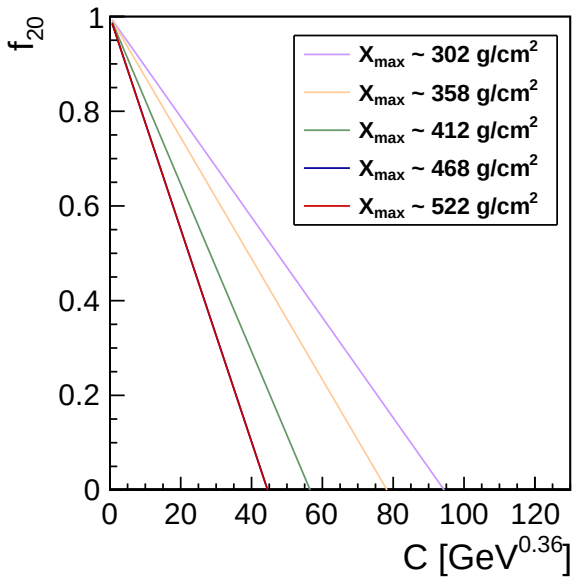


Figure 12 Calibration lines (f_{20}, C) for several ranges of $X_{\rm max}$ and with $S_{\rm em} \sim 200\,\mathrm{GeV}$.

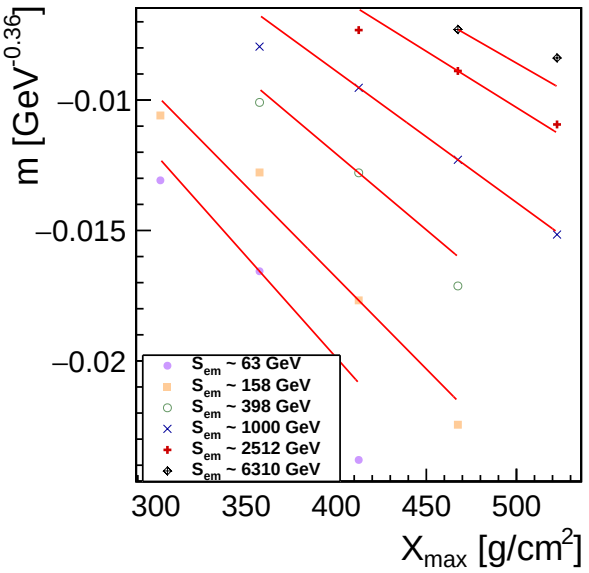


Figure 13 Correlation of the slope of the calibration lines represented in 12 with $X_{\rm max}$, for different $S_{\rm em}$ bins (see caption).

icle[3]. So we will keep the linear approximation using $b_m = 0.011\,\mathrm{GeV}^{-0.36}$ for all $S_{\rm em}$.

[3]For the energies considered in this article, most shower events have $X_{\rm max}$ values around $\sim 400 \pm 100\,\mathrm{g\,cm^{-2}}$. A shower with $X_{\rm max} \gtrsim 500\,\mathrm{g\,cm^{-2}}$ would have its $X_{\rm max}$ buried in the ground while a shower with $X_{\rm max} \lesssim 200\,\mathrm{g\,cm^{-2}}$ would only reach the ground if it strongly fluctuates.

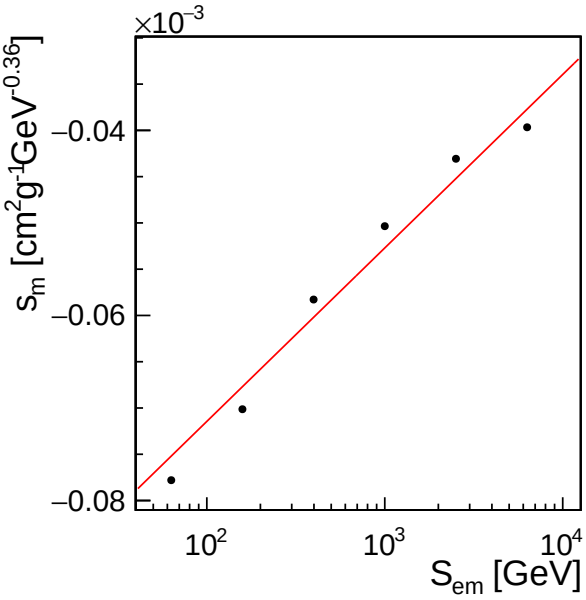


Figure 14 Correlation of the slope s_m of the m calibration lines represented in fig 13 as a function of $S_{\rm em}$.

Finally, the slope s_m of the lines represented in figure 13 are shown in figure 14 as a function of $\log(S_{\rm em})$. A linear correlation is found between s_m and $\log(S_{\rm em})$. As such, one can write,

$$f_{20} = 1 + m(X_{\rm max}, S_{\rm em})\, C(f_{20}, X_{\rm max}, S_{\rm em})\,, \qquad (10)$$

and,

$$m(X_{\rm max}, S_{\rm em}) = b_m + [s_{m0} + s_{m1}\,\log(S_{\rm em}/\mathrm{GeV})]\, X_{\rm max} \qquad (11)$$

The best achieved parametrization with the above equation is shown in figure 14, with parameters $s_{m0} = -1.1 \times 10^{-4}\,\mathrm{GeV}^{-0.36}\,\mathrm{g}^{-1}\mathrm{cm}^2$ and $s_{m1} = 1.87 \times 10^{-5}\,\mathrm{GeV}^{-0.36}\,\mathrm{g}^{-1}\mathrm{cm}^2$.

Finally,

$$C(f_{20}, X_{\rm max}, S_{\rm em}) = \frac{1 - f_{20}}{-\left(b_m + [s_{m0} + s_{m1}\log(S_{\rm em})]\, X_{\rm max}\right)} \qquad (12)$$

and,

$$E_0^{(2)} = S_{\rm em} + C(f_{20}, X_{\rm max}, S_{\rm em})\,(S_{\rm em})^{\beta}, \qquad (13)$$

which is our best estimator for the primary energy.

Using in the above parametrization, A_0 (see section 2) as the estimator of $S_{\rm em}$ and $X^R_{\rm max}$ (see section 3) as the estimator of $X_{\rm max}$, an energy resolution below 30 % and 20 % were obtained at 1 TeV and 10 TeV, respectively.

Using instead the real $X_{\rm max}$ and $S_{\rm em}$, these energy resolutions improve to about 8% and 4% . These results may be considered as the *ultimate* resolutions. The difference between the estimated resolutions and the *ultimate* resolutions are driven, in the TeV region, mainly by the resolution of the $S_{\rm em}$ estimator. Indeed, a resolution of 12% on the parameter A_0, the $S_{\rm em}$ estimator, even considering the simulated $X_{\rm max}$ value, would translate into a resolution on $E_0^{(2)}$ of 22% .

In figure 15 are shown (full red thick line) the estimated energy ($E_0^{(2)}$) resolution as a function of the primary energy. For comparison, the equivalent resolutions obtained applying the constant C calibration ($E_0^{(1)}$), full red thin line, defined by equation 9, or using systematically the $X^0_{\rm max}$ estimator (dashed red thin line) are also shown. It is also shown the resolutions that would be obtained using the simulated value of $X_{\rm max}$ (dashed blue line), or the simulated value of $S_{\rm em}$ (pointed blue line) or finally using both simulated values (blue thin line).

These results are obtained considering an ideal detector. The degradation factors due to the detector effects are briefly discussed in the next section.

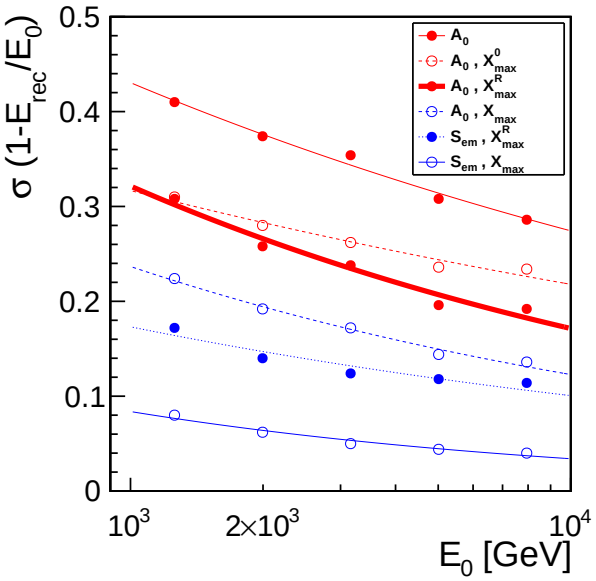


Figure 15 Energy resolution as a function of the primary energy. The red lines correspond to constant C coefficients (thin) and $C(X_{\rm max}, f_{20})$ coefficients, using $X^R_{\rm max}$ (thick) or $X^0_{\rm max}$ (dashed); resolutions obtained with simulated values are also shown for comparison (blue lines) : simulated value of $X_{\rm max}$ (dashed), simulated value of $S_{\rm em}$ (pointed) and both simulated values (thin).

5 Discussion and Conclusions

In this article, new and innovative methods for the determination of the total electromagnetic energy at the ground, of the slant depth of the maximum of the longitudinal profile and, of the primary energy were proposed. In particular, as much as we know, it is the first time that the steepness in the core region of the cumulative function of the energy arriving at the ground is used as a determinant factor to obtain the energy calibration constants.

The obtained results are very promising and can open new physics avenues. The improvement on the energy resolution has, as a direct consequence, a meaningful increase of the sensitivity of the observatories. The obtained resolutions on $X_{\rm max}$, yet to be confirmed for cosmic ray shower, would allow very interesting studies on the development of the shower, namely on the characterization of the mass composition of hadronic cosmic rays. This shall be focus of a future publication.

These results, even if obtained considering an ideal detector, are quite robust as they rely only on the estimation of the electromagnetic energy at the ground, $S_{\rm em}$ and, of the slant depth of the maximum of the longitudinal profile, $X_{\rm max}$, which may be, in a first-order approximation, also obtained from the $S_{\rm em}$. Typically, a region of a few tens of meters around the core and an energy at the ground of several tens of GeV have to be measured to be able to efficiently apply the proposed algorithms.

The estimation of $S_{\rm em}$ is thus the critical factor to be able to achieve a good resolution on the reconstruction of the primary gamma-ray energy. Further progress may be envisaged using more sophisticated $S_{\rm em}$ estimators, like the one suggested by the cumulative function parametrization described in equation 2, or applying, for instance, machine learning techniques.

All the present results were obtained using vertical showers. Inclined showers would imply lower energies at the ground. For instance, at 1 TeV an inclined 30° shower would deposit at the ground around 20% less than a vertical shower of the same energy (see, for instance [17]). Therefore, at lower energies, the energy resolutions will be worse, scaling with $S_{\rm em}$. Taking LHAASO [13], as an example, it was shown that for 10 TeV gamma induced showers, there is a degradation in the reconstructed energy resolution of $\sim 20\%$ when moving from showers with zenith angle $\theta \in [0°, 20°]$ to

$\theta \in [20°, 35°]$. It should be noted that the ability to measure higher energies may improve as the probability of the depth of shower maximum to be above the ground surface increases.

A detailed study of the performance of the new reconstruction methods for a specific Wide Field of View Gamma Ray Observatory is out of the scope of this work. Nevertheless, it is important to discuss briefly possible factors that would contribute to the degradation of the results obtained in the previous sections. Most of these effects are mainly critical for primary energies below a few hundreds of GeV, corresponding to energies at the ground of a few tens of GeV, where a detailed design and simulation of the detectors would be mandatory.

The following factors need to be considered:

- **The amount of signal (p.e.) generated in each station**
  The electromagnetic energy deposited in each station may be converted into photoelectrons (p.e.) using as conversion factors $n_{\mathrm{Photon}} \sim 40\,F$ p.e./GeV where F is, following [18], a scale factor. $F = 1$ corresponds to the existing performance at HAWC. Much higher values of F were found in LATTES end-to-end simulations [19]. Fluctuations may then be generated using a Poisson distribution.
  Anyway, for energies at 1 TeV or above the total signal per event is above several thousands of p.e., even for the more conservative F scale factors. The uncertainty in the measurements of F_{50} and F_{20} is then, at lower energies of the order of just a few % and at higher energies negligible, which in any case will be translated at most in a minor increase of the obtained energies resolutions.
- **The precision on the location of the shower core**
  The reconstructed shower core position should, for each event, be smeared by a few meters following the resolutions quoted in [19] (3 m at 1 TeV, $<$ 1 m at 10 TeV). This would introduce distortions in the cumulative functions which would correspond to an increase of at most a few % in the value of the resolution of the A (S_{em}) estimator.
- **The finite dimension of the compact array region of the observatory**
  The distance of the core position to the border of the compact array region of the observatory will determine the fraction of the event footprint at the ground that would be measured. However, it is possible to imagine more sophisticated methods, using, for instance, neural networks, to make a reasonably accurate estimation of the S_{em} even in the case where there is only a partial containment of the shower footprint in the required region around the core.
- **The time resolution at each detector station**
  Time resolutions better than 2 ns are crucial for good angular resolutions [20]. Assuming that the detectors would comply with a 2 ns time resolution, the particle arrival times should be smeared and the X^1_{max} estimator (see section 3) re-computed. Once again, this effect should be mainly important for lower energies; at higher energies, above a few TeV, there will be a high number of hit stations and the curvature fit will be more robust. Nevertheless, giving up the possibility to compute, for each event, the curvature of the shower front, the systematic use of the X^0_{max} estimator would have only impact at energies above a few TeV degrading the energy resolutions at 10 TeV from 20% to 25%, as shown by the dashed red line in figure 15.

The results obtained, representing such a considerable improvement concerning the presently quoted energy resolutions of the existing or planned Wide Field of View Gamma-Ray Observatories, clearly will encourage detailed simulations and studies on the applicability of the proposed methods.

Acknowledgements We would like to thank to A. Bueno, A. De Angelis and J. Vicha for all the useful discussions and carefully reading the manuscript. The authors thank also for the financial support by OE - Portugal, FCT, I. P., under project PTDC/FIS-PAR/29158/2017. R. C. is grateful for the financial support by OE - Portugal, FCT, I. P., under DL57/2016/cP1330/cT0002.

References

1. B. Rossi, K. Greisen, Revs. Mod. Phys. **13**, 240 (1941). DOI 10.1103/RevModPhys.13.240
2. K. Greisen, Progr.Cosmic Ray Physics **3**, 1 (1956)
3. T.K. Gaisser, A.M. Hillas. Reliability of the method of constant intensity cuts for reconstructing the average development of vertical showers. Proc. 15th International Cosmic Ray Conference Plovdiv, Vol 8 353 (1977)
4. J. Montanus. Intermediate models for longitudinal profiles of cosmic showers. arXiv:1106.1073 [astro-ph.HE],(2011)
5. S. Andringa, R. Conceição, M. Pimenta, Astroparticle Physics **34**, 360 (2011). DOI 10.1016/j.astropartphys.2010.10.002
6. J. Aleksic, et al. (MAGIC Collaboration), Astroparticle Physics **72**, 76 (2016). DOI 10.1016/j.astropartphys.2015.02.005
7. V. Joshi, J. Hinton, H. Schoorlemmer, R. López-Coto, R. Parsons, JCAP **01**, 012 (2019). DOI 10.1088/1475-7516/2019/01/012
8. A. Abeysekara, et al., The Astrophysical Journal **881**, 134 (2019). DOI 10.3847/1538-4357/ab2f7d
9. A. Aab, et al., Phys. Rev. D **96**(12), 122003 (2017). DOI 10.1103/PhysRevD.96.122003

10. D. Heck, J.N. Capdevielle, G. Schatz, T. Thouw, F.K. Gmbh. Corsika: A monte carlo code to simulate extensive air showers," report fzka 6019, forschungszentrum karlsruhe (1998)
11. J. Kamata, K.and Nishimura, Progress of Theoretical Physics Supplement **6**, 93 (1958). DOI 10.1143/PTPS.6.93
12. K. Kawata, T. Sako, M. Ohnishi, M. Takita, Y. Nakamura, K. Munakata, Experimental Astronomy **44** (2017). DOI 10.1007/s10686-017-9530-9
13. F. Aharonian, et al., (2020). ArXiv:2010.06205
14. W. Weibull, Journal of Applied Mechanics **18**, 293 (1951)
15. A. Calabrese Melcarne, G. Marsella, D. Martello, L. Perrone, S. Sbano, in *32nd International Cosmic Ray Conference*, vol. 1 (2011), vol. 1, pp. 66–69. DOI 10.7529/ICRC2011/V01/0402
16. T. Stanev, C.P. Vankov, F. Halzen. Muons in gamma showers. In NASA. Goddard Space Flight Center 19th Intern. Cosmic Ray Conf., Vol. 7 p 219-222 ,(1985)
17. A. Abeysekara, et al., Astropart. Phys. **35**, 641 (2012). DOI 10.1016/j.astropartphys.2012.02.001
18. W. Hofmann. Impact of altitude and Cherenkov photon detection efficiency on the energy threshold of SWGO-like arrays. HAP-20-003
19. P. Assis, et. al., Astropart.Phys. **99**, 34 (2018). DOI 10.1016/j.astropartphys.2018.02.004
20. W. Hofmann, Astropart. Phys. **123**, 102479 (2020). DOI 10.1016/j.astropartphys.2020.102479